NANO LETTERS

2005
Vol. 5, No. 7
1519−1523

Electrical Transport through a Single Nanoscale Semiconductor Branch Point

Yi Cui,[†,‡] Uri Banin,[‡,§] Mikael T. Björk,[‡,||] and A. Paul Alivisatos*[,†,‡]

Department of Chemistry, University of California and Materials Sciences Division, Lawrence Berkeley National Laboratory, Berkeley, California 94720

Received June 7, 2005

ABSTRACT

Semiconductor tetrapods are three-dimensional (3D) branched nanostructures, representing a new class of materials for electrical conduction. We employ the single-electron transistor approach to investigate how charge carriers migrate through single nanoscale branch points of tetrapods. We find that carriers can delocalize across the branches or localize and hop between arms depending on their coupling strength. In addition, we demonstrate a new single-electron transistor operation scheme enabled by the multiple branched arms of a tetrapod: one arm can be used as a sensitive arm-gate to control the electrical transport through the whole system.

Electrical transport through nanocrystals,[1] molecules,[2,3] nanotubes,[4,5] and nanowires[6,7] displays novel quantum phenomena. These can be studied using the single-electron transistor approach to successively change the charge state by one, to reveal charging energies, electronic level spacings, and coupling between electronic, vibrational, and spin degrees of freedom. The advent of colloidal synthesis methods that produce branched nanostructures[8,9] provides a new class of material that can act as conduits for electrical transport in hybrid organic−inorganic electrical devices such as light-emitting diodes[10−12] and solar cells.[13,14] Already, the incorporation of branched nanostructures has yielded significant improvements in nanorod/polymer solar cells, where the specific pathways for charge migration can have a significant impact on device performance.[14] Progress in this area requires an understanding of how electrons and holes migrate through individual branch points. For instance, do charges delocalize across the branches or do they localize and hop between arms? Here we employ the single-electron transistor approach to investigate the simplest 3D branched nanostructure, the semiconductor tetrapod, which consists of a pyramidal shaped zincblende-structured "core" with four wurzite-structured arms projecting out at the tetrahedral angle.

Monodisperse CdTe tetrapods with arms 8 nm in diameter and 150 nm in length were synthesized as reported previously.[8] The tetrapods dispersed in toluene were deposited onto ∼10-nm-thick Si_3N_4 dielectrics with alignment markers and a back gate (see Supporting Information). A tetrapod spontaneously orients with one arm pointing perpendicularly away from the substrate and three arms projecting down toward the surface. Individual 60-nm-thick Pd electrodes were placed by EBL onto each of the three arms downward so that there are four terminals (three arms and a back gate) as shown schematically in the top inset of Figure 1. The bottom inset of Figure 1 shows a typical scanning electron micrograph (SEM) of the devices. The center brighter spot is due to the fourth arm pointing up away from the substrate, although its controlled breaking is possible.[15] The separation between the metal electrodes and the tetrapod branch point ranges from 30 to 80 nm in our devices. The devices were loaded into a He^4-flow cryostat for low-temperature (∼5K) electrical measurements.

Typical curves of current (I) as a function of source−drain bias voltage (V) through arm pair 1−2 (Figure 1, bottom inset) at different back-gate voltage (V_g) while keeping the third arm floating are presented in the main panel of Figure 1. The $I-V$ curves show a strongly suppressed conductance at small V values and a steplike increase of I at high V values, suggesting single-electron charging behavior. The size of the zero conductance gaps could be changed reversibly by V_g. Pair 2−3 and 1−3 show similar behavior. Measurements are reproducible with time (Supporting Information). More than 20 working devices fabricated from 5 different independent processes have been measured. Their characteristics fall into two different categories (see below).

The differential conductance ($\partial I/\partial V$) as a function of V and V_g for these two categories is plotted in Figure 2a and c. Focusing now on Figure 2a, the zero-conductance regions

* To whom correspondence should be addressed. E-mail: alivis@berkeley.edu.
† University of California, Berkeley.
‡ Lawrence Berkeley National Laboratory.
§ Permanent address: Institute of Chemistry and the Center for Nanoscience and Nanotechnology, The Hebrew University of Jerusalem, Jerusalem 91904, Israel.
|| Current address: Solid State Physics/Lund University, P.O. Box 118, SE-221 00, Lund Sweden.

10.1021/nl051064g CCC: $30.25
Published on Web 06/18/2005

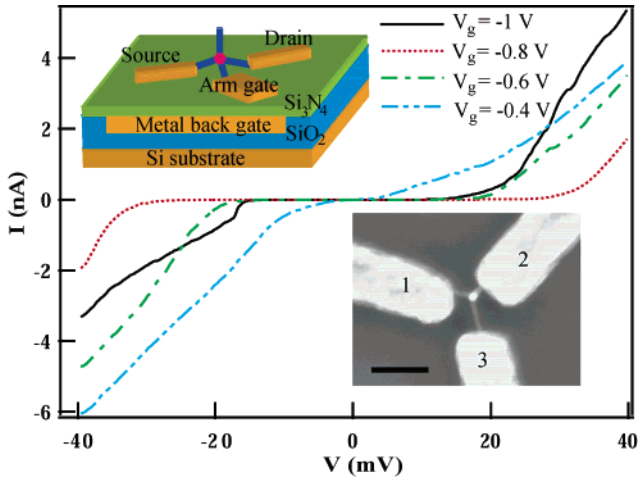

Figure 1. Scheme of tetrapod single-electron transistor and $I-V$. Main panel, $I-V$ at different back-gate voltages indicated with a different color and line style measured at $T = 5$ K. Top inset, the device schematic structure, in which three arms of a tetrapod are contacted with small metal electrodes and the fourth arm points vertically away from the substrate. The red spot indicates the tetrapod branch point. Bottom inset, a SEM image of a tetrapod contacted with three Pd electrodes labeled as 1, 2, and 3. Scale bar, 100 nm.

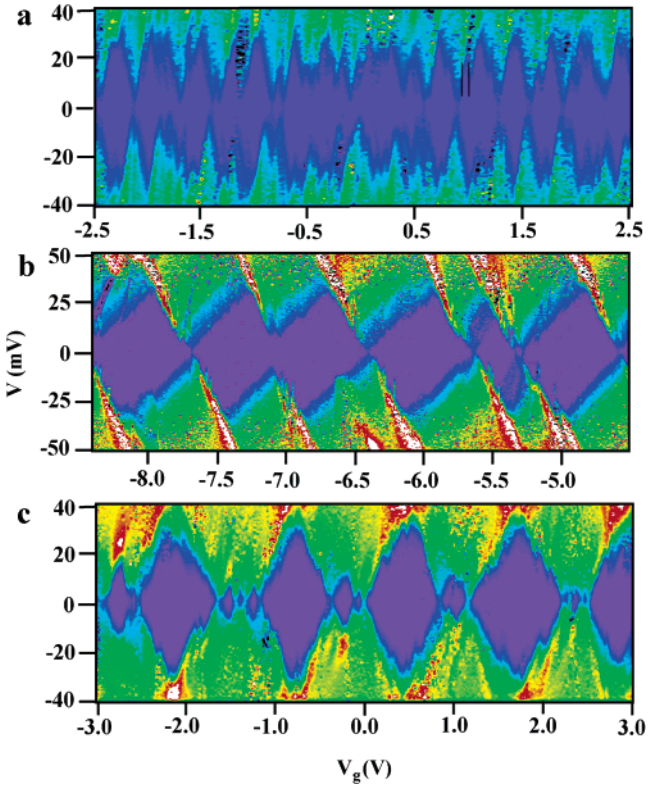

Figure 2. Plots of $(\partial I/\partial V)$ as function of V and V_g at $T = 5$ K. a, A tetrapod showing hopping. The two black lines mark two of the sawteeth. b, A CdSe nanorod. The two sudden shifts along V_g have been corrected. The raw data is shown in Supplementary Figure 2. c, A tetrapod showing delocalization. The color scale: purple, zero; light blue, 5 nS in a; green, 25 nS in b; green, 150 nS in c. The back-gate coupling efficiency is different: ~16% in a and ~4% in b and c because of the variation of dielectrics thickness.

(purple) are now bound by higher conductance ones (light blue). Most notably, distinct from single dot charging, which has well-defined zero-conductance diamonds arranged one by one along the V_g axis, the tetrapod shows many overlapping diamonds to the extent that the boundary of individual Coulomb diamonds exhibits a sawtooth rather than a smooth structure. This is a clear signature of single-electron hopping in a system of weakly coupled quantum dots.[16] In the tetrapod, a coupled quantum dot system can form because the electron is transported through the arm−branch point−arm in series. Further support of this conjecture is afforded by the addition energy, E_{add} of ~30 meV obtained from the maximum size of V in the diamonds, which matches the charging energy of the tetrapod branch point with a size ~10 nm. Here $E_{add} = E_c + \Delta E$, where E_c is the Coulomb charging energy, $E_c = e^2/C$ and ΔE is the energy level spacing. For estimation of the order of magnitude, the capacitance, C, of a branch point can be approximated by sphere self-capacitance, $2\pi\epsilon\epsilon_0 D$, where ϵ takes the average (4.5) of Si_3N_4 and vacuum dielectric constants, ϵ_0 is the vacuum permittivity, and D is the branch point diameter. This gave an upper bound E_c value of 60 meV because other capacitance contributions can reduce this value. The ΔE is ~5 and 45 meV from the effective-mass model for the holes and electron, respectively. Transport is most likely through the valence band and does not contribute to E_{add} significantly (see Supporting Information). The calculated E_{add} is thus consistent with experiments. This addition energy cannot be explained by charging the much larger whole tetrapod as a single quantum dot, which should display a charging energy of only a few millielectronvolts. The observed value is also consistent with previous electrical transport[1] and scanning tunneling microscopy measurements[17] of quantum dots of size similar to the tetrapod core size. Other devices in the same category also give a narrow range of addition energies, 30−45 meV, further confirming it is mainly due to the branch point. A second addition energy scale observed in the data can be estimated from the separation between the adjacent sawteeth, which is typically ~60 mV (between the two black lines in Figure 2a), and when taking into account the gate coupling efficiency translates into a charging energy of ~10 meV, corresponding to the size of a single arm (estimated charging energy ~5 meV, see Supporting Information).[6]

Mechanisms other than electronic quantum dot and rod coupling are less likely to contribute significantly to the differential conductance spectra shown here. First, the vibration and twisting motions of tetrapods are at gigahertz or microelectronvolts, which cannot account for the observed addition energy, although they might exert some effects on fine structure outside of the Coulomb diamonds. A second possibility is that surface-localized surface defect states could play a role. The tetrapods here show little or no band edge luminescence and trap states within the band gap act as nonradiative centers.[18] However, localized surface states are less likely to play a role in the transport measurements compared to states that are more delocalized. Further, the Fermi level remains in the valence band (see Supporting Information) during measurements, and defect states are less likely to play an important role at this energy. However, we

observed sudden shifts of Coulomb charging diamonds along the V_g axis once every few hours at 5 K. The measurements after temperature cycles still show similar sawtooth charging patterns with the same addition energy. To resolve this matter, we have investigated simple nanorods, which should not show coupling phenomena but do have surface states. Figure 2b shows a similar measurement performed on a single quantum rod with dimensions of 4 by 50 nm. Here a smooth set of Coulomb diamonds is seen, indicating one addition energy scale characteristic of a single quantum dot. The value of the estimated charging energy is consistent with the rod dimension (see Supporting Information). This observation provides strong additional support for our assignment of the sawtooth structure in the tetrapod case to single-electron transport through the artificial molecule arm−branch point−arm system.

Although 80% of the tetrapod devices exhibited sawtooth transport characteristics, in 20% we observed a different behavior as shown in Figure 2c. Here a large diamond with an additional energy of ~30 meV and two or three small ones with additional energies of 3−15 meV alternate along the V_g axis. These features cannot be explained within a single-dot charging picture because E_c and ΔE of the whole tetrapod as a dot are too small. Instead, these are expected for charge carrier delocalization within the whole tetrapod in the limit of the strongly coupled arm−branch point−arm system similar to the lithographically patterned dots on 2D electron gas.[19] Large diamonds correspond to the states with a large probability of a charge on the branch point and little on the arms because it is more confined; small diamonds are the states with a large probability of a charge on the arms and little on the branch point because it is more spread out.

To further differentiate the two transport regimes in tetrapods, let us examine them more closely (Figure 3a): (1) In the hopping case, the branch point and arms interact electrostatically with small tunnel conductance.[16] The charge carriers are localized on the individual branch points or arms and are incoherently transferred or hop between them. This regime can be modeled, to the simplest approximation, as three Coulomb charging energy ladders[20] (Figure 3a, left) connected in series, which represent the arm−branch point−arm transport pathway. The other two arms can also cause some effect, but their effect is not considered for qualitative analysis. Current can flow only if the charging levels line up within the window of V or the thermal fluctuation. (2) In the delocalization case, the coupling between the electronic states in the branch points and the arms is strong. The charge carrier can tunnel many times between the branch point and the arms and can be considered to coherently delocalize over the whole tetrapod. The Coulomb charging states can be modeled using a single energy ladder (Figure 3a, right) formed by the hybridized bonding and antibonding states of the branch point and the arm charging states. Current can flow without the requirement of level lineup.

Bias or temperature dependence provides clear evidence to differentiate the two coupling mechanisms. Figure 3b plots I as a function of V_g at different V values for the hopping case. Notably, when the bias is increased gradually from 1 to 10 mV, the number of Coulomb oscillation peaks increases. This behavior can be explained by the three-energy-ladder model in the hopping limit. Because the three energy ladders are distributed randomly, at small bias (1 mV, Figure 3b, red), the probability to have all three levels line up within the narrow energy window is small and thus the appearance of Coulomb oscillations peaks is sparse and appears stochastic.[20] Indeed in the gate scan range in Figure 3b, there is no peak at all. At larger bias (5 mV, Figure 3b, green), the probability of line-up is increased and the peaks appear in the form of groups with a large separation between them, indicating capacitive coupling phenomena. When the bias is larger than the arm charging energy (10 mV, Figure 3b, black), there are always levels lining up within the bias window for current flow. Thus, the number of groups of peaks increases further. At even higher bias, the number of peaks within each group can increase because of conduction through excited states.

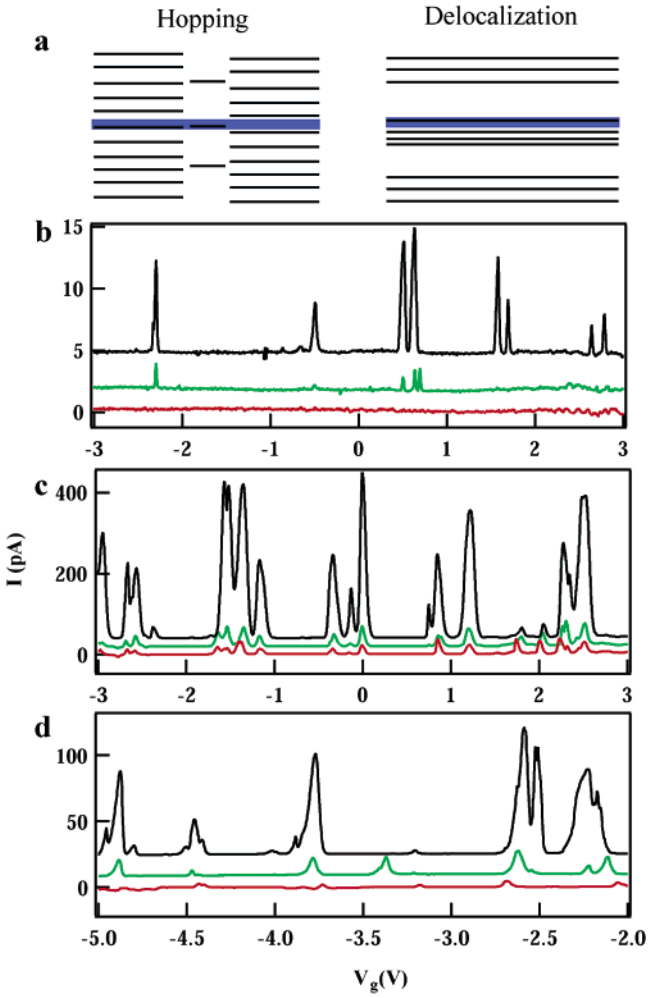

Figure 3. Comparison of the hopping and delocalization couplings. a, Hopping and delocalization models. The blue stripes indicate V or the thermal energy window. b−d, Plots of I versus V_g at $T = 5$ K and different V for hopping (b), delocalization (c) and nanorod (d). The red, green, and black curves represent $V = 1$, 5, and 10 mV in b; 0.5, 1, and 5 mV in c and d. The curves are shifted in the vertical axis for clarity. b was taken from a device different from Figure 2a. c and d were taken from the same device as Figure 2c and b, respectively.

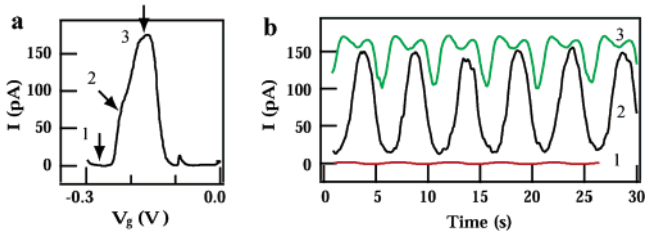

Figure 4. Integrated tetrapod transistors at 5 K. a, I versus V_g at $V = 10$ mV. The arrows indicate the three V_g values for current at: 1, blockade; 2, half-maximum; 3, peak. b, I versus time with $V =$ 10 mV and 0.2 Hz sinusoidal AC voltage applied to the third arm at the three V_g values in a. The rms of the AC voltage is 40 mV for curves 1 and 2, 100 mV for 3. The $I-V$ measurements through the third arm show a gap of 150 mV, presumably because of the defect formation during process and the AC voltage is small enough to avoid current leakage.

In contrast, the delocalization case shows very different V-dependent behavior (Figure 3c). The Coulomb peaks also appear in groups but because of the hybridization of large and small charging energies, the peak number does not change when V is changed from 0.5, 1−5 mV, consistent with the single delocalized energy ladder. Compared to hopping and delocalization in tetrapods, similar measurements in single nanorods (Figure 3d) show the same number of individual peaks at low bias except that there are peak splittings at high bias (black) because of excited-state conduction. Temperature has a similar effect in controlling the transport window size and supports the above explanation (Supporting Information Figure 3).

Weak hopping coupling with negligible interdot tunneling can be described by the orthodox theory of the Coulomb blockade.[21,22] The important parameters (capacitances, resistances) of the single-electron transistor circuit have been extracted (Supporting Information Figure 4) from the charge stability diamond plot as shown in Figure 2a. Thus, the weak coupling energy[16] in the hopping limit ($E_{c-hopping}$) between the tetrapod branch point and the arm can be calculated, $E_{c-hopping} = e^2/C_{point-arm}\,(C_{point}C_{arm}/C_{point-arm}^2 - 1)^{-1}$, where e is the electron charge, $C_{point-arm}$ is the capacitance between a branch point and an arm, and C_{point} and C_{arm} are the total branch point and the total single arm capacitance, respectively. Given the $C_{point-arm}$, C_{point}, and C_{arm} values of 2.4, 5.3, and 26.7 aF from the transistor circuit, respectively (Supporting Information Figure 4), we obtained an $E_{c-hopping}$ of ∼3 meV. We note that the two arms coupled parallel to the transport pathway modify this coupling energy only in an insignificant manner.

In comparison, we also estimated the strong coupling energy in the delocalization limit ($E_{c-delocalization}$) for the plot shown in Figure 2c. As a simple approximation, the coupling energy can be assigned as the spread range of the same group of Coulomb oscillation peaks as shown in Figure 3c. Given a spread of 0.34−0.5 V in gate axis and a gate coupling efficiency, we obtained an $E_{c-delocalization}$ of 15−20 meV, which is 5−7 times the estimated value of $E_{c-hopping}$. These coupling energy scales in tetrapod are 1 order of magnitude larger than those of lithographically patterned quantum dot molecules,[19] consistent with the much smaller size of the tetrapods.

There may be several sources for the interesting observation of both hopping and delocalization in tetrapods. Clearly this shows a variation of barrier heights at the arm−branch point−arm junctions between different tetrapod devices. A first possible source is strain induced by the mechanical bending of the arms close to the junction between the arms and the branch point. Mechanical strain can induce lattice distortion and thus change the band gap of a semiconductor.[23] Different degrees of bending will lead to band-gap variations. Previous SEM studies provide clear evidence of arm bending in most because of capillary force attraction when the solvent dries during deposition on the substrate.[24] Recent atomic force microscopy and transmission electron microscopy studies also confirm that strain is most significant near the junction point of the tetrapod (private communications). To make a rough estimate of an energy barrier induced by mechanical bending, we simply treat the case as pure bending of a beam. Assuming a reasonable bending radius of curvature, $R = 40$ nm, the strain $= r/R$ is determined to be 10%, where r is the radius of the arm. Taking the shear deformation potential[23] of CdTe ∼1.4 eV, we get a 140-meV energy barrier, which is significant at cryogenic temperature. This is consistent with the fact that most of our samples show hopping coupling although the bending radius of curvature can vary widely in different tetrapods. The delocalization coupling requires that the arm bending is little with $R > \sim 1\mu$m, which can also happen in some tetrapods. Another possible source for the barriers is the existence of stacking faults and change of growth angle at the arm−branch point interface, which may also vary between different tetrapods. Further experiments are required to clarify these two sources and are currently under investigation. For example, tuning the mechanism between the two coupling extremes continuously by controlling the mechanical deformation might be achievable by changing the interaction between substrate and tetrapod electrostatically, and/or by atomic force microscope manipulation.

A coupled tetrapod also provides a unique integrated multiterminal structure for new electrical device configurations. We have explored this opportunity by the third arm gating. We measured I across two of the arms at $V = 10$ mV while scanning the back gate, V_g, to locate a Coulomb oscillation peak as shown in Figure 4a. We fixed V at 10 mV and V_g at a specific value (position 1, 2, or 3) indicated by the arrow and applied 0.2 Hz AC voltage to the third arm. The current was recorded with time (Figure 4b) and with voltage (Supporting Information Figure 5). At position 1 of V_g, the current was in a blockaded state and modulating the arm gate gives little changes of current (Figure 4 curve 1). In contrast, at position 2 where the current rises with V_g, the current can be changed by the arm gate from the peak value to almost zero. When V_g is fixed at position 3, the modulation of current with the arm gate shows two peaks within the 5-s period, consistent with two passes of the Coulomb oscillation peak in one period. From comparing

the change of the back-gate and arm-gate voltage for the same amplitude of the current modulation, the arm-gate coupling efficiency is estimated to be ~70% of that of the back-gate efficiency. These preliminary studies suggest that the main gating mechanism is mainly through the third arm. Another gating mechanism from direct electrostatic interaction of the arm-gate metal electrode and the tetrapod at a 30-nm distance would have a lower gating efficiency than the observed one and plays a less important role, although the future study is needed to subtract out its contribution in a quantitative way.

Acknowledgment. We thank Professor David Goldhaber-Gordon for invaluable suggestions and discussion. We also thank the National Center for Electron Microscopy at Lawrence Berkeley National Lab and the UC Berkeley Microfabrication Lab for use of their facility. Y.C. thanks the Miller Institute for a fellowship. M.B. thanks the Office of Naval Research for support. This work was supported by the Director, Office of Science, Office of Basic Energy Sciences, Division of Materials Sciences and Engineering, the Laboratory Directed Research and Development Program of Lawrence Berkeley National Laboratory of the U.S. Department of Energy, by Department of Defense Advanced Research Projects Agency (DARPA), and by DARPA/ Nanosys, Inc. through the Flexible Nanocomposite Photovoltaics Project.

Supporting Information Available: Methods and supporting data. This material is available free of charge via the Internet at http://pubs.acs.org.

References

(1) Klein, D. L.; Roth, R.; Lim, A. K. L.; Alivisatos, A. P.; McEuen, P. L. *Nature* **1997**, *389*, 699−701.
(2) Park, J.; Pasupathy, A. N.; Goldsmith, J. I.; Chang, C.; Yaish, Y.; Petta, J. R.; Rinkoski, M.; Sethna, J. P.; Abruña, H. D.; McEuen, P. L.; Ralph, D. C. *Nature* **2002**, *417*, 722−725.
(3) Liang, W.; Shores, M. P.; Bockrath, M.; Long, J. R.; Park, H. *Nature* **2002**, *417*, 725−729.
(4) Tans, S. J.; Devoret, M. H.; Dai, H.; Thess, A.; Smalley, R. E.; Geerligs, L. J.; Dekker, C. *Nature* **1997**, *386*, 474−477.
(5) Bockrath, M.; Cobden, D. H.; McEuen, P. L.; Chopra, N. G.; Zettl, A.; Thess, A.; Smalley, R. E. *Science* **1997**, *275*, 1922−1925.
(6) Cui, Y.; Duan, X.; Hu, J.; Lieber, C. M. *J. Phys. Chem. B* **2000**, *104*, 5213−5216.
(7) Thelander, C.; Mårtensson, T.; Björk, M. T.; Ohlsson, B. J.; Larsson, M. W.; Wallenberg, L. R.; Samuelson, L. *Appl. Phys. Lett.* **2003**, *83*, 2052−2054.
(8) Manna, L.; Milliron, D. J.; Meisel, A.; Scher, E. C.; Alivisatos, A. P. *Nat. Mater.* **2003**, *2*, 382−385.
(9) Milliron, D. J.; Hughes, S. M.; Cui, Y.; Manna, L.; Li, J.; Wang, L. W.; Alivisatos, A. P. *Nature* **2004**, *430*, 190−195.
(10) Colvin, V. L.; Schlamp, M. C.; Alivisatos, A. P. *Nature* **1994**, *370*, 354.
(11) Coe, S.; Woo, W.-K.; Bawendi, M.; Bulovic, V. *Nature* **2002**, *420*, 800−803.
(12) Tessler, N.; Medvedev, V.; Kazes, M.; Kan, S.; Banin, U. *Science* **2002**, *295*, 1506−1508.
(13) Huynh, W. U.; Dittmer, J. J.; Alivisatos, A. P. *Science* **2002**, *295*, 2425−2427.
(14) Sun, B.; Marx, E.; Greenham, N. C. *Nano Lett.* **2003**, *3*, 961−963.
(15) Liu, H.; Alivisatos, A. P. *Nano Lett.* **2004**, *4*, 2397−2401.
(16) van der Wiel, W. G.; De Franceschi, S.; Elzerman, J. M.; Fujisawa, T.; Tarucha, S.; Kouwenhoven, L. P. *Rev. Mod. Phys.* **2003**, *75*, 1−22.
(17) Banin, U.; Millo, O. *Annu. Rev. Phys. Chem.* **2003**, *54*, 465−492.
(18) Nirmal, M.; Brus, L. *Acc. Chem. Res.* **1999**, *32*, 407−414.
(19) Crouch, C. H.; Livermore, C.; Westervelt, R. M.; Campman, K. L.; Gossard, A. C. *Appl. Phys. Lett.* **1997**, *71*, 817−819.
(20) Ruzin, I. M.; Chandrasekhar, V.; Levin, E. I.; Glazman, L. I. *Phys. Rev. B* **1992**, *45*, 13469−13478.
(21) Grabert, H.; Devoret, M. H. *Single Charge Tunneling: Coulomb Blockade Phenomena in Nanostructures*; Plenum Press: New York, 1992; Chapter 1−3.
(22) Wasshuber, C. *Single Electronics*; Spring-Verlag/Wien: New York, 2001; Chapter 2.
(23) Mathieu, H.; Allegre, J.; Chatt, A.; Lefebvre, P.; Faurie, J. P. *Phys. Rev. B* **1988**, *38*, 7740−7748.
(24) Cui, Y.; Björk, M. T.; Liddle, J. A.; Sönnichsen, C.; Boussert, B.; Alivisatos, A. P. *Nano Lett.* **2004**, *4*, 1093−1098.

NL051064G